A MULTI-MODE STATE-SPACE DYNAMIC MODEL FOR PYROFUSION NEUTRON SOURCES

A.M. Darbyshire[†*] and K.D. Atkinson[†]
[†] Defence Academy of the United Kingdom,
[*] University of Cambridge
alice.darbyshire990@mod.uk

ABSTRACT

Pyrofusion neutron sources are compact, low power systems which may be capable of producing short intense pulses of neutrons from D-D fusion reactions. The neutron pulse duration has been too short for use as a continuous wave source, and too long for application in interrogation techniques. However, initial analysis of pyrofusion dynamics has indicated the potential to manipulate the pulse characteristics through system control. This paper introduces the development of state-space multimode system models in MATLAB/Simulink that may be used to support the predictability and control of the neutron pulse. Preliminary examples of frequency-domain studies, stability analysis and time-domain simulations are reported.

Key Words: pyrofusion neutron source, frequency response, state-space, MATLAB/Simulink

1 INTRODUCTION

Previous research groups have focused efforts on the development of the hardware to increase the neutron flux [1], [2], [3]. It is anticipated that the pyrofusion devices will require substantial control efforts to make these systems useful. The pyrofusion dynamic models under development in MATLAB/Simulink could potentially be used for:

1. Estimation of pyrofusion system dynamic response, stability and performance.

2. Determination of controllable pyrofusion dynamics and controllability boundaries.

3. Indication of the type of additional system equalization desirable to achieve better control.

4. Identification of the maximum forcing function bandwidth compatible with reasonable control action.

2 MATHEMATICAL MODEL

The pyrofusion source comprises pyroelectric crystals in a single or paired arrangement; the work presented in this paper focuses on a single crystal shown in Fig.1 attached to a thermoelectric heater/cooler. These components are contained within a vacuum chamber which is partially filled with low pressure Deuterium gas and contains a deuterated target. When the pyroelectric crystal is thermally cycled a change in bound surface charge develops on the exposed polarised face. Through this pyroelectric effect the crystal generates high voltages and a strong electric field in the chamber. The electric field is capable of ionising the deuterium gas and accelerating the ions into the deuterated target to produce a pulse of neutrons.

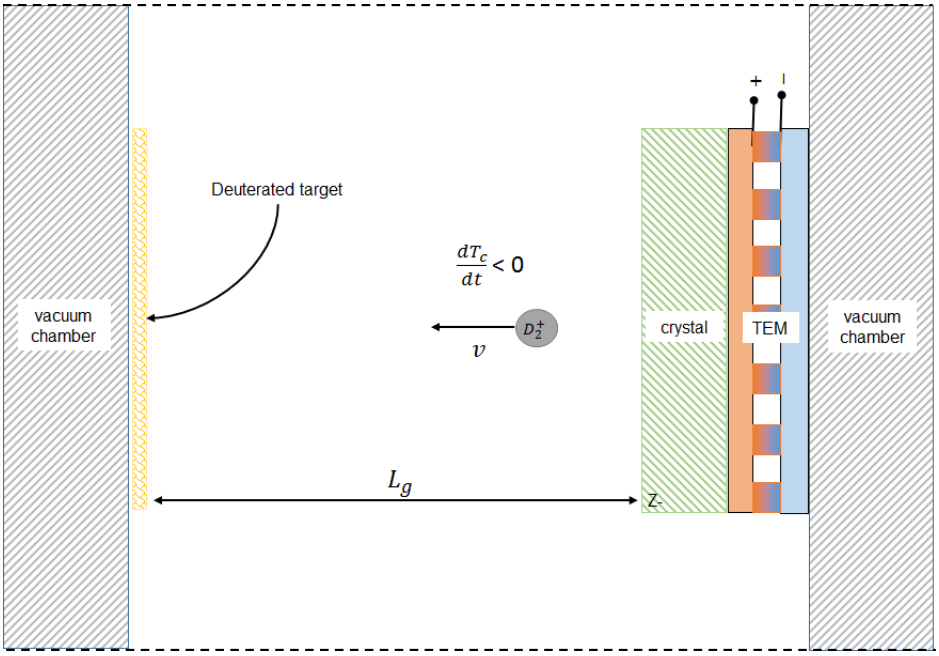

(a) Single crystal orientation in vacuum chamber

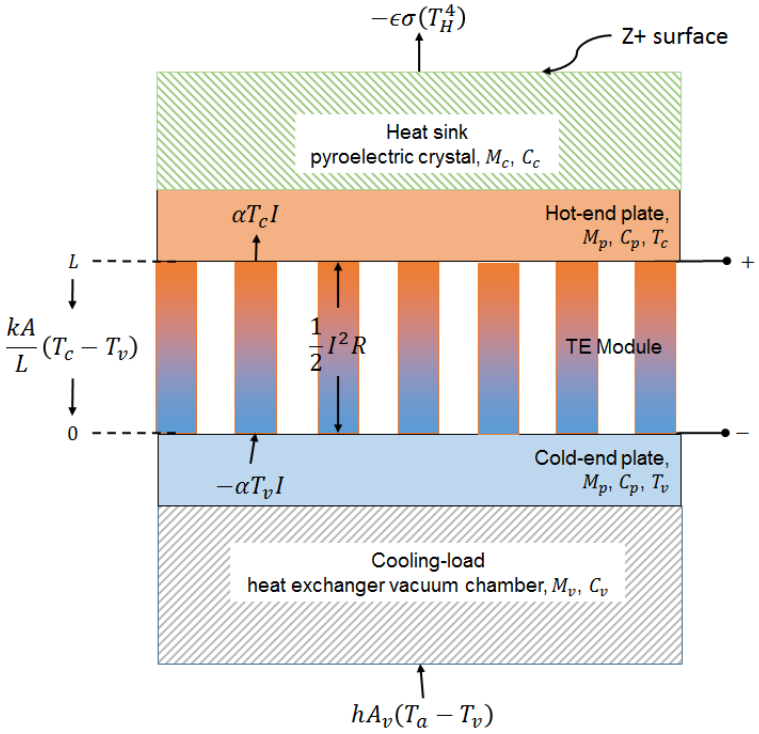

(b) Temperature distribution across crystal

Figure 1. Schematic of single crystal system

2.1 Thermal subsystem equations

With reference to Fig.1, during a heating cycle, heat is absorbed at the vacuum chamber cooling-load and conducted to the cold-end plate of the thermoelectric module (TEM); it is then pumped to the hot-side of the module and into the crystal. The temperature distributions inside the cold-end plate and the vacuum chamber can be assumed to be uniform [4]. The describing equation for the energy balance to the cold-end plate (subscript p) and the vacuum chamber cooling-load (subscript v) can be written as

$$\left(\mathrm{M_v C_v + M_p C_p}\right)\frac{\mathrm{dT_v}}{\mathrm{dt}} = -\mathrm{I\alpha T_v} + \mathrm{hA_v}\left(\mathrm{T_a - T_v}\right) + \frac{\mathrm{k_p A_c}}{\mathrm{L_p}}\left(\mathrm{T_c - T_v}\right) + \frac{\rho_\mathrm{p} \mathrm{L_c}}{2\mathrm{A_c}}\mathrm{I}^2 \quad (1)$$

where M_v is the mass of the vacuum chamber cooling-load [kg],
C_v is the heat capacity of the vacuum chamber cooling-load [J/kg-K],
M_p is the mass of the cold-end plate of thermoelectric module [kg],
C_p is the heat capacity of the cold-end plate of thermoelectric module [J/kg-K],
T_v is temperature of the vacuum chamber (i.e. the cold side of the TEM) [K],
I is the applied current to the thermoelectric module [amps],
α is the Seeback coefficient of thermoelectric material [V/K],
T_a is the temperature of the external environment [K],
k_p is the mean thermal conductivity of the thermoelectric material [W/K],
A_c is the total cross-sectional area of the crystal; and is equal to the cross-sectional area for heat transfer across the thermoelectric material [m^2]
ρ_p is the bulk resistivity of the thermoelectric material [$\Omega - \mathrm{m}$] and,
L_p is the length of the thermoelectric elements [m].

The energy balance to the crystal heat-sink (subscript c) and the hot-end plate (subscript p) as a whole leads to

$$\left(\mathrm{M_c C_c + M_p C_p}\right)\frac{\mathrm{dT_c}}{\mathrm{dt}} = \mathrm{I\alpha T_c} - \frac{\mathrm{k_p A_c}}{\mathrm{L_p}}\left(\mathrm{T_c - T_v}\right) - \epsilon\sigma \mathrm{A_c T_v^4} + \frac{\rho_\mathrm{p} \mathrm{L_c}}{2\mathrm{A_c}}\mathrm{I}^2 \quad (2)$$

where M_c is the mass of the crystal heat-sink [kg],
C_c is the heat capacity of the crystal heat-sink [J/kg-K],
T_c is the temperature of the crystal (i.e. the hot side of the TEM) [K],
ϵ is the emissivity of the crystal heat-sink,
σ is the Stefan-Boltzmann constant [W/m^2K^4].

Equations 1 and 2 are the describing equations for the thermal dynamics of the thermoelectric cooler, crystal heat-sink, and chamber cooling-load in the pyroelectric system. The equations are highly non-linear due to the temperature dependence of the physical properties, the resistive heat and the Peltier effect.

2.2 Thermal to pyroelectric subsystem equations

Changes in bulk crystal temperature alter the lattice spacing of non-symmetrically located ions within pyroelectric crystals, such as Lithium Tantalate ($LiTaO_3$). The ion displacement varies the spontaneous polarization of the crystal, producing a displacement current I_c parallel to the crystal's polar axis. The pyroelectric crystal thermal to electrical conversion may be simply represented as [5]

$$\mathrm{I_c} = \gamma\, \mathrm{A_c}\, \frac{\mathrm{dT_c(t)}}{\mathrm{dt}} \quad (3)$$

where $\gamma = 190\,\mu\,C/K - m^2$ is the pyroelectric coefficient for $LiTaO_3$. The pyroelectric current I_c to crystal voltage V_c may then be expressed as

$$\mathrm{C_c}\frac{\mathrm{dV_c(t)}}{\mathrm{dt}} + \frac{\mathrm{V_c(t)}}{\mathrm{R_c}} = \mathrm{I_c(t)} \tag{4}$$

where the electrical time constant of the crystal, τ_e is

$$\tau_\mathrm{e} = \mathrm{R_c C_c} \tag{5}$$

The generated crystal surface charge may be calculated by

$$\frac{\mathrm{dQ_c}}{\mathrm{dt}} = \mathrm{c}\frac{\mathrm{dV_c(t)}}{\mathrm{dt}} \tag{6}$$

where c is the system capacitance, expressed as

$$\mathrm{c} = \epsilon_\mathrm{o}\,\epsilon_\mathrm{cr}\,\mathrm{A_c/L_c} + \mathrm{c_{para}} \tag{7}$$

and ϵ_0 is the standard permittivity of the vacuum; $\epsilon_c = 47$ is the relative permittivity of the $LiTaO_3$ and $L_c = 0.01\,m$ is the length of the crystal. The parasitic capacitance in typically sized systems is $c_{para} \approx 0.8\,pF$; this is due to the chamber walls and electrical wires [3].

2.3 System Linearisation

Using a small-perturbation analysis a linearised equation set for a typical the pyrofusion device can be formed. The variables are considered to be the summation of a steady-state value (denoted by $\bar{X}$) and a small change (denoted by $\tilde{X}$) about that operating point, i.e.

$$\begin{aligned} \mathrm{T_c(t)} &= \overline{T_c}(\mathrm{t}) + \widetilde{T_c}(\mathrm{t}) \\ \mathrm{T_v(t)} &= \overline{T_v}(\mathrm{t}) + \widetilde{T_v}(\mathrm{t}) \\ \mathrm{I(t)} &= \bar{I}(\mathrm{t}) + \tilde{I}(\mathrm{t}) \\ \mathrm{V_c(t)} &= \overline{V_c}(\mathrm{t}) + \widetilde{V_c}(\mathrm{t}) \end{aligned} \tag{8}$$

Equation set 8 can be substituted into equations 1, 2, and 4. Taking constant properties for k_p, ρ_p, C_p, C_v, C_c, α, and γ, with the preceding considerations, and eliminating steady-state and high order terms; the following equations, 9, 10 and 11 may be realised.

$$\left(\mathrm{M_v C_v} + \mathrm{M_p C_p}\right)\dot{\widetilde{T_v}} = -\alpha\,\bar{I}\,\widetilde{T_v} - \alpha\overline{T_v}\tilde{I}\,\frac{\mathrm{k_p A_c}}{\mathrm{L_p}}\left(\widetilde{T_c} - \widetilde{T_v}\right) - \mathrm{hA_v}\widetilde{T_v} + \frac{\rho_\mathrm{p}\bar{I}}{2\mathrm{L_p}}\,\tilde{I} \tag{9}$$

$$\left(\mathrm{M_c C_c} + \mathrm{M_p C_p}\right)\dot{\widetilde{T_c}} = \alpha\,\bar{I}\,\widetilde{T_c} + \alpha\overline{T_c}\tilde{I}\,\frac{\mathrm{k_p A_c}}{\mathrm{L_p}}\left(\widetilde{T_c} - \widetilde{T_v}\right) - 3\,\epsilon\sigma\mathrm{A_c}\,\overline{T_c^3}\,\widetilde{T_c} + \frac{\rho_\mathrm{p}\bar{I}}{2\mathrm{L_p}}\,\tilde{I} \tag{10}$$

$$(\mathrm{R_c C_c})\dot{\widetilde{V_c}} = \gamma\,\mathrm{A_c}\,\mathrm{R_c}\dot{\widetilde{T_c}} - \widetilde{V_c} \tag{11}$$

3 SYSTEM REPRESENTATION IN STATE-SPACE

The linear time-invariant system of Eqns. 9, 10 and 11 may be represented in state-variable form as a set of first-order differential equation, expressed as vector-matrix differential equations of the form

$$\dot{x}(\mathrm{t}) = \mathrm{f}\,[\,\mathrm{x(t), u(t), t}\,] \tag{12}$$

where x(t) is an n-dimensional state vector, u(t) is an r-dimensional control vector, f is the system function and t is time. With consideration to the physical signals present in the pyrofusion system an appropriate state vector may be chosen as

$$x(t) = \left[\, \tilde{T}_v(\mathrm{t})\ \tilde{T}_c(\mathrm{t})\ \tilde{V}_c(t) \right]^T \tag{13}$$

Taking derivatives of the state set in Eqn. 13 yields the state variable representation as equation set 14}.

$$\begin{aligned} \dot{x_1} &= \tau_{\mathrm{v}}^{-1}\left[\, -\alpha \bar{I}\tilde{T_v} + \mathrm{c}_2(\tilde{T_c} - \tilde{T_v}) - \mathrm{hA_v}\,\tilde{T_v} + (\mathrm{c}_1\bar{I} - \alpha\,\overline{T_v})\,\tilde{I}\,\right] \\ \dot{x_2} &= \tau_{\mathrm{c}}^{-1}\left[\, \alpha\,\bar{I}\,\tilde{T_c} - \mathrm{c}_2\big(\tilde{T_c} - \tilde{T_v}\big) - 3\epsilon\sigma \mathrm{A_c}\,\overline{T_c^3}\,\widetilde{T_c} + (\mathrm{c}_1\bar{I} + \alpha\,\overline{T_c}\,)\,\tilde{I}\right] \\ \dot{x_3} &= \tau_{\mathrm{e}}^{-1}\,\tau_{\mathrm{c}}^{-1}\gamma\,\mathrm{A_c R_c}\big[\,\alpha\,\bar{I}\,\tilde{T_c} - \mathrm{c}_2\big(\tilde{T_c} - \tilde{T_v}\big) - 3\epsilon\sigma \mathrm{A_c}\,\overline{T_c^3}\,\widetilde{T_c} + (\mathrm{c}_1\bar{I} + \alpha\,\overline{T_c}\,)\,\tilde{I}\big] - \tau_{\mathrm{e}}\,\tilde{V_c} \end{aligned} \tag{14}$$

where $\tau_v = M_v C_v + M_p C_p$ is the vacuum chamber thermal time constant, $\tau_c = M_c C_v + M_p C_p$ is the crystal thermal time constant, $\tau_e = R_c C_c$ is the crystal electrical time constant. Two system constants, $c_1 = \frac{\rho_p}{2 l_p}$ and $c_2 = k_p \frac{A_c}{l_p}$ are the electrical and thermal constants respectively. The vector-matrix form of Eqn. set 14 may expressed in the form

$$\begin{aligned} \dot{x}(\mathrm{t}) &= \mathrm{Ax(t)} + \mathrm{Bu(t)} \\ \mathrm{y(t)} &= \mathrm{Cx(t)} + \mathrm{Du(t)} \end{aligned} \tag{15}$$

where the system matrix is

$$A = \begin{bmatrix} \tau_v^{-1}(-\alpha\ \bar{I} - c_2 - hA_v) & \tau_v^{-1}c_2 & 0 \\ \tau_c^{-1}c_2 & \tau_c^{-1}(\alpha\,\bar{I} - c_2 - 3\,\epsilon\sigma A_c\,\overline{T_c^3}) & 0 \\ \tau_e^{-1}\tau_c^{-1}\gamma A_c R_c c_2 & \tau_e^{-1}\tau_c^{-1}\gamma A_c R_c(\alpha\,\bar{I} - c_2 3\,\sigma A_c\,\overline{T_c^3}) & -\tau_e^{-1} \end{bmatrix} \tag{16}$$

and the control input matrix is

$$B = \begin{bmatrix} \tau_v^{-1}(\,c_1\,\bar{I} - \alpha\,\overline{T_v}) \\ \tau_c^{-1}(\,c_1\,\bar{I} + \alpha\,\overline{T_c}) \\ \tau_e^{-1}\tau_c^{-1}\gamma A_c R_c(\,c_1\,\bar{I} + \alpha\,\overline{T_c}) \end{bmatrix} \tag{17}$$

A suitable output vector for system analysis is

$$y = [\tilde{T_v} \quad \tilde{T_c} \quad \tilde{V_c} \quad \tilde{q} \quad \tilde{n}]^T \tag{18}$$

During the heating phase the system generates deuterons. Assuming that all the surface charge is converted into ions q, the required output matrix C is

$$C = \begin{bmatrix} 1 & 0 & 0 \\ 0 & 1 & 0 \\ 0 & 0 & 1 \\ 0 & 0 & -\frac{c}{1.6\times10^{-19}} \\ 0 & 0 & 0 \end{bmatrix} \tag{19}$$

where the charge of a deuteron is $1.6 \times 10^{-19}\,C$. The feed-through vector D=0. During the cooling cycle, neutrons can be generated from D-D fusion as the deuterons are accelerated into a deuterated target, and one of two possible reactions may occur:

$$ {}_1^2H \ + \ {}_1^2H \ \rightarrow \ {}_2^3\mathrm{He} \ (0.82 \text{ MeV}) \ + \ {}_0^1n \ (2.45 \text{ MeV})\} \quad (50 \ \%) $$

$$ {}_1^2H \ + \ {}_1^2H \ \rightarrow \ {}_1^3T \ (1.01 \text{ MeV}) \ + \ p^+ \ (3.02 \text{ MeV})\} \quad (50 \ \%) \tag{20} $$

A suitable output matrix for analysis of the dominant characteristics during this phase of the cycle is:

$$ C = \begin{bmatrix} 1 & 0 & 0 \\ 0 & 1 & 0 \\ 0 & 0 & 1 \\ 0 & 0 & 0 \\ 0 & 0 & \frac{1}{2} N_d \sigma \frac{c}{1.6 \times 10^{-19}} \end{bmatrix} \tag{21} $$

where N_d is the target density of deuterium atoms per unit volume and σ is the total integrated cross section for D-D fusion.

4 PARAMETER VARIATION STUDY

A parameter variation study may be conducted in MATLAB using a sampling tuneable model. The selected operating point variations for this study are given by Eqn. 22 evaluating the system for all combinations of these values results in an array of models. Each entry in the array is a state-space model that represents the system evaluated at the corresponding operating points.

$$ \begin{aligned} \bar{T_c} &= [233 \quad 253 \quad 293 \quad 313 \quad 343] \\ \bar{T_v} &= [233 \quad 253 \quad 293 \quad 313 \quad 343] \\ \bar{I} &= [0 \quad 1 \quad 2 \quad 3] \end{aligned} \tag{22} $$

The resulting pyroelectric potential frequency response plots presented in Fig2 indicate that;

1. Variations in vacuum chamber temperature operating point have the least effect on the responsivity.

2. In the intermediate range of frequencies, near the maximum crystal potential magnitude the responsivity decreases slightly with decreasing crystal temperature.

3. The input current operating point variations have greatest effect in the low frequency range.

4. In typical pyrofusion experiments it has been observed that $\approx 80 \ keV$ is required for a reasonable ion production [1]. The plots indicate that a suitable input frequency range between $\approx 3 \times 10^{-5}$and $\approx \ 10^{-1} \ rad/s$ may be required for the successful operation of the particular system geometry studied.

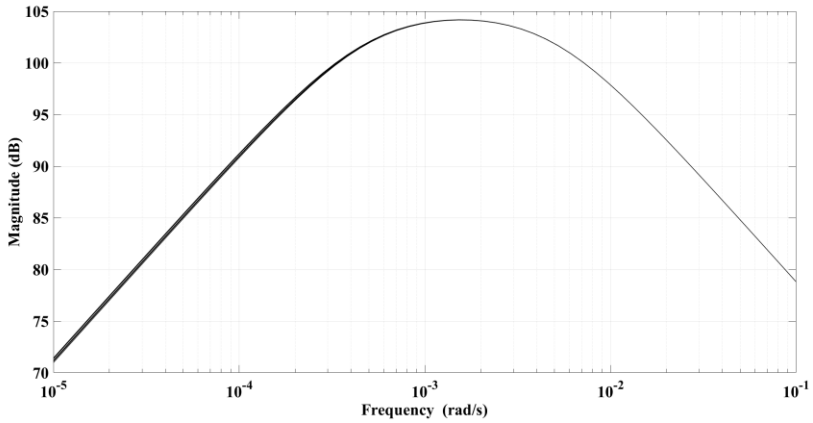

a) Effect of model vacuum chamber temperature $\overline{T_v}$ operating point variations.

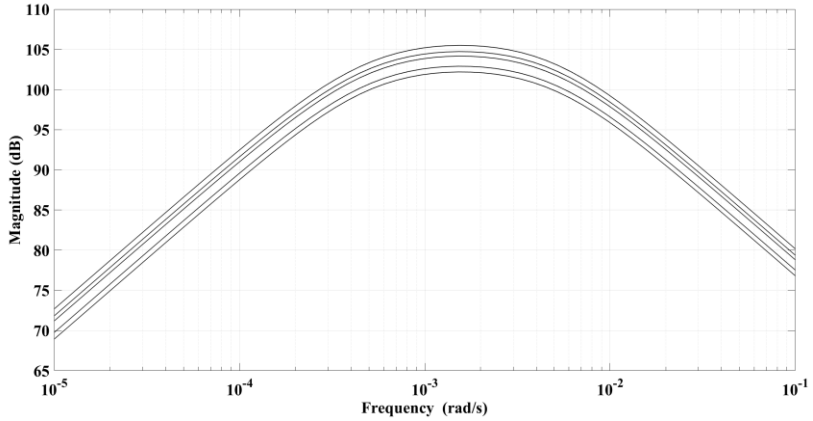

b) Effect of model vacuum chamber temperature $\overline{T_c}$ operating point variations.

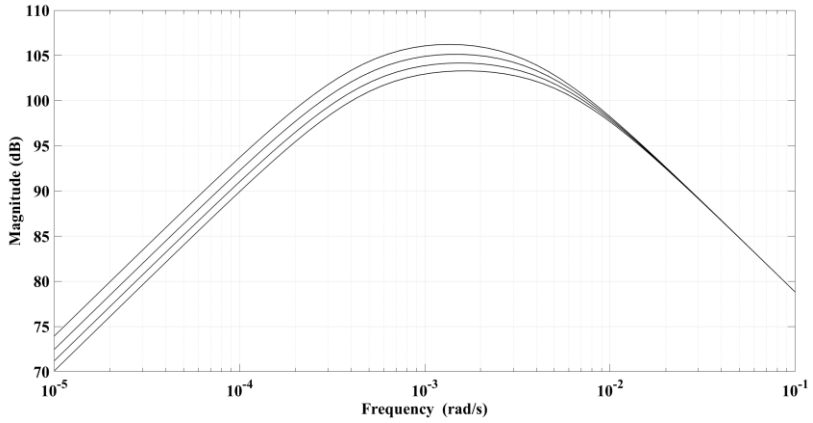

c) Effect of model vacuum chamber temperature $\bar{I}$ operating point variations.

Figure 2: Effect of model operating point variations on pyroelectric crystal potential response.

The system response may be interpreted in terms of a trajectory in the state-space, giving additional physical meaning to the time response of the system. The time response in the phase plane is generated by starting at an initial condition. The shape of the trajectory depends on the eigenvalues of the system.

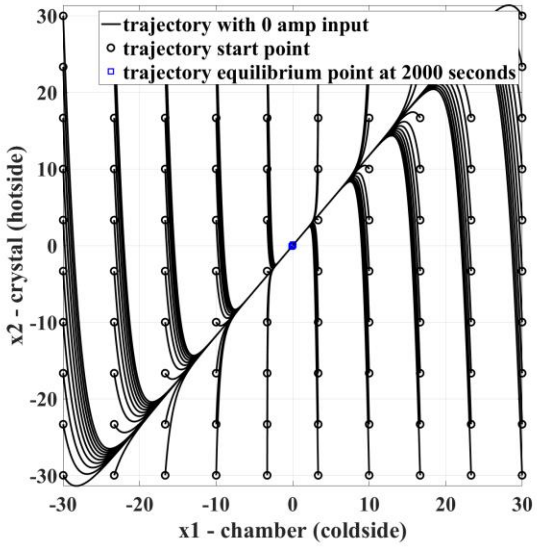

a) Phase-planes trajectories of the thermal system

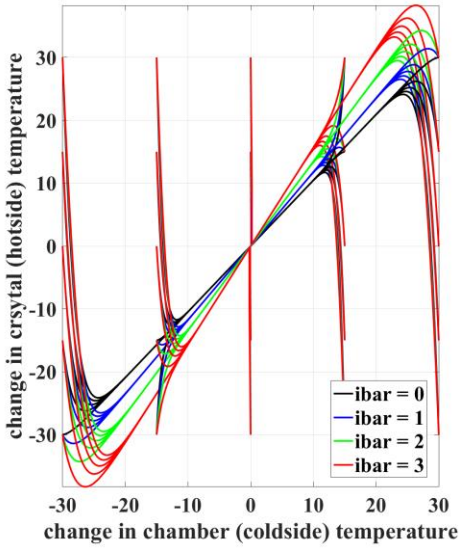

b) Effect of model $\bar{I}$ operating point variations

Figure 3: Example phase-planes trajectories of the thermal system

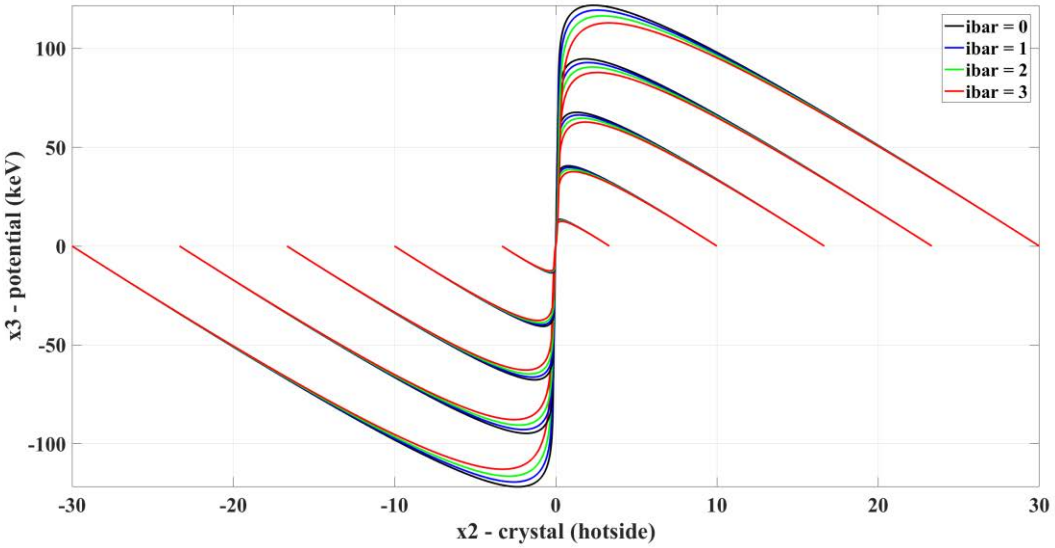

a) Effect of model $\bar{I}$ operating point variations on crystal temperature-potential trajectories

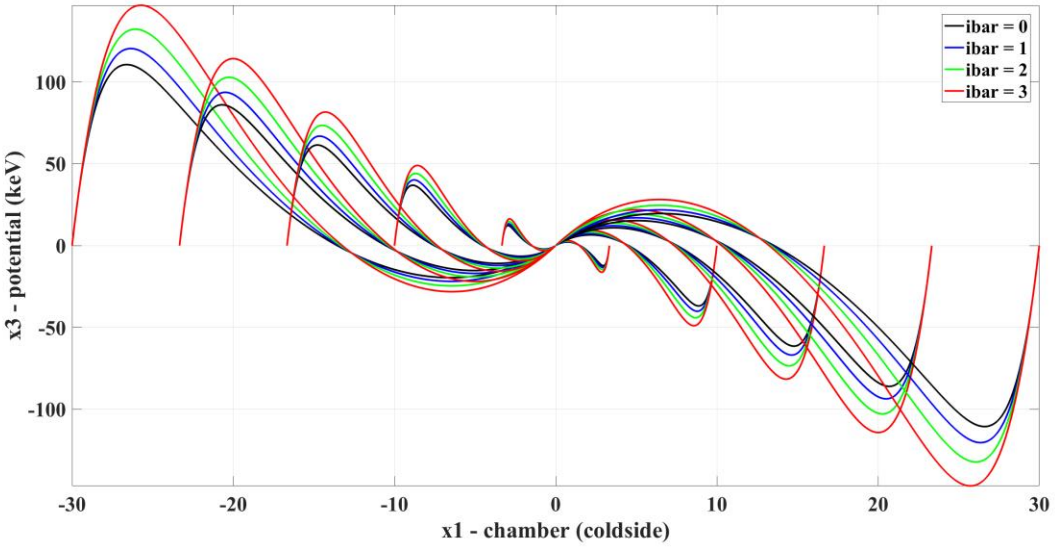

b) Effect of model $\bar{I}$ operating point variations on chamber temperature-potential trajectories

Figure 4: Example phase-planes trajectories of the pyroelectric system

The system phase-plane plots presented in Fig.3 and Fig.4 show;

1. The phase-plane portraits for system temperature changes, shown in Fig.3 are stable nodes, indicating that the eigenvalues of the thermal system are real and negative.

2. Variation of the model input current operating point $\bar{I}$ does not affect the stability of the system.

3. The phase-plane portraits in Fig.4 showing system temperature-potential changes are also found to be a stable nodes, indicating that the eigenvalues of this system are real and negative.

4. Theoretically, a crystal temperature change of $\approx 30^{o}C$ could generate a potential of $\approx 100\ keV$. In experiments around twice this temperature change is required.

5. Changes in the vacuum chamber temperature effect the crystal and lead to changes in potential.

6. The current operating point value, $\bar{I}$ is representative of an active heat pump in the thermal system. The phase-plane trajectories shown in Fig.4a indicate that this action opposes the generation of potential for crystal temperature state. The reverse effect can be observed for vacuum chamber temperature state in Fig.4b.

5 LINEAR PARAMETER VARYING (LPV) MODEL

The physical system exhibits distinct non-linear behavioural modes corresponding to the heating and cooling phases of the operational thermal cycle. By considering an array of the linear state-space models it becomes possible to treat these non-linear dynamics as a single system whose coefficients change as a function of a set of scheduling parameters which determine which mode is active under given conditions. The effect of operating point variations on frequency response may then be investigated using a Linear Parameter Varying (LPV) model of the system. An example LPV model of the pyrofusion system implemented in Simulink is shown in Fig.5.

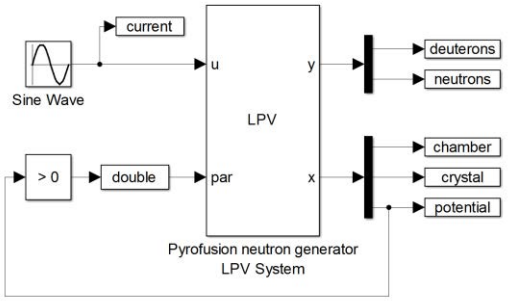

Figure 5. Example block diagram of a pyrofusion LPV Simulink model.

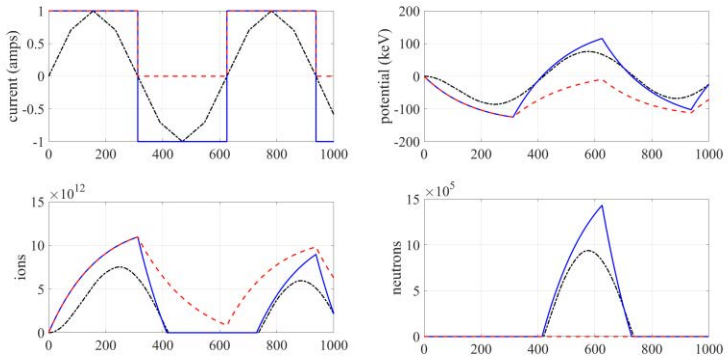

Figure 6. Example of the LPV model response for various current input signals.

The LPV block contains an array of state-space models, with crystal potential as the scheduling parameter. Fig.6 shows an example of the model response during sinusoidal, square

and pulse thermal cycle operations. For the purpose of comparison, all signals have amplitude current input of 1 amp and frequency of $10^{-2}\ rad/s$. The sinusoidal and square wave signals represent the ability to force cool the crystal using the current switching capabilities of a thermoelectric cooler control system. These preliminary simulations indicate there may be a forced cooling operational requirement at this frequency.

6 CONCLUSIONS

The simulations in MATLAB/Simulink of a simple pyrofusion neutron source model demonstrate the possibilities of investigation into the dynamic characteristics using methods of control engineering theory. Extensions to the current model and future research may include:

1. Simulation and analysis of the effects system non-linearities such as charge saturation, ionisation dead-band, and pyroelectric hysteresis on system stability and controllability.

2. State-variable feedback controller design to minimise the effect of disturbances during cycling and saturation within the system.

3. Closed-loop optimal-control law design with consideration of system constraints and time-varying system parameter behaviours.

4. Extension of the model to include multi-crystal arrangements and optimised combined heating/cooling cycles.

7 ACKNOWLEDGMENTS

Any views expressed herein are those of the author(s) and do not necessarily represent those of Defence Academy of the United Kingdom.

8 REFERENCES

1. B. Naranjo, J. Gimzewski, and S. Putterman, "Observation of nuclear fusion driven by a pyroelectric crystal," *Nature*, **434**, pp.1115–1117 (2005).

2. J. Geuther, "Enhanced Neutron Production From Pyroelectric Fusion," *Applied Physics Letters*, **90**, 174103 (2007).

3. D. Gillich, "Particle Acceleration with Pyroelectric Crystals," *PhD Dissertation, Rensselear Polytechnique Institute* (2009).

4. B. Huang and C. Duang, "System dynamic model and temperature control of a thermoelectric cooler," *International Journal of Refrigeration*, **23**, pp.197–207 (2000).

5. R.L. Byer and C.B. Roundy, "Pyroelectric Coefficient Direct Measurement Technique and Application to an NSEC Response Time Detector," *IEEE Trans. Sonics and Ultrasonics*, **3**, pp.333–338 (1972).

6. A. Odon, "Modelling and Simulation of the Pyroelectric Detector Using MATLAB/Simulink," *Measurement Science Review*, **10,6**, pp.195–199 (2010).